Runaway relativistic electron avalanche seeding in the Earth's atmosphere

B. E. Carlson,[1] N. G. Lehtinen,[1] and U. S. Inan[1]

[1] Relativistic runaway electron avalanches (RREAs) occur when relativistic electrons undergo avalanche multiplication when driven by electric fields. The RRE avalanche has been studied extensively, but existing results typically assume a rudimentary source of seed relativistic electrons. Here we focus on the seeding process and simulate effective seeding efficiencies for various seed particle types, energies, and geometries. Including known results from cosmic ray physics, we calculate total seed particle distributions and their statistical fluctuations and use the seeding efficiency results to determine the total number of effective RREA seed particles at various points in the atmosphere. The results indicate that effective seed flux is quite large with only moderate statistical fluctuations.

1. Introduction

[2] Runaway relativistic electron avalanche (RREA) is an avalanche multiplication process proposed to occur in moderate electric fields in gasses [e.g., *Gurevich et al.*, 1992; *Gurevich and Zybin*, 2001]. As the lower dynamic friction on relativistic electrons lowers the minimum electric field required for RREA approximately an order of magnitude lower than the conventional breakdown threshold, RREA has been suggested as the underlying mechanism for several processes in the Earth's atmosphere, such as lightning initiation [e.g., *Dwyer*, 2005; *Marshall et al.*, 2005; *Gurevich et al.*, 1999], impulsive radio emissions [e.g., *Tierney et al.*, 2005], sprite and blue jet formation [e.g., *Lehtinen et al.*, 1999; *Babich et al.*, 2007; *Roussel-Dupré and Gurevich*, 1996], and terrestrial gamma ray flashes [e.g., *Dwyer and Smith*, 2005; *Inan and Lehtinen*, 2005; *Lehtinen et al.*, 1999]. RREA has been treated in detail by Monte Carlo simulations, from which properties such as the avalanche growth rate, speed of propagation, the influence of feedback, and resulting gamma ray emissions have been determined for certain conditions [e.g., *Coleman and Dwyer*, 2006; *Babich et al.*, 2005; *Lehtinen et al.*, 1996], but many aspects of RREA are still poorly understood including the source and nature of the driving electric fields involved, the initiation of RREA within these fields, the extent of the avalanche growth possible, and the ultimate observable effects. We herein focus on the initiation process of the avalanche.

[3] Avalanche multiplication occurs whenever the electric field exceeds the threshold for RREA but cannot begin without the presence of seed relativistic electrons, requiring at least one energetic particle to initiate the process. Under normal conditions, the Earth's atmosphere has many such energetic particles resulting partly from radioactive decay but largely from cosmic rays (CRs) and the extensive air showers (EASs) of secondary particles they produce. However, the details of how energetic cosmic ray secondary particles initiate RREA are dependent on many factors. For instance, seed electrons moving in different directions relative to the electric field or with different energies will behave differently in initiating RREA, as will different CR EAS secondary particle types such as photons, electrons, positrons, and muons. We here focus on the initiation and seeding of RREA under such circumstances, ignoring the more complex and situation-dependent source processes such as thermal runaway under large fields or feedback from ongoing RREA.

[4] Previous treatments of RREA have largely assumed a population of ~ 1 MeV seed electrons and instead focused on the avalanche growth. Assumed seed populations are typically based on approximations of the average cosmic ray secondary flux [e.g., *Lehtinen et al.*, 1999] or on the maximum number of secondary particles present in a single EAS [e.g., *Gurevich and Zybin*, 2004; *Inan and Lehtinen*, 2005]. While straightforward and useful, such assumptions depend on the length and time scales relevant to each particular case and should be verified. More detailed treatments of the energetic particles which are present and capable of initiating RREA can only be undertaken in connection with sufficiently detailed treatments of the cosmic ray primary and secondary flux.

[5] In this paper we present detailed Monte Carlo simulations of the cosmic ray secondary flux distributions relevant to RREA seeding, including statistical fluctuations. We further present Monte Carlo simulations of the RREA initiation process and present effective seeding efficiencies for various seeding geometries, particle types, and energies.

[1] Space, Telecommunications, and Radioscience Laboratory, Electrical Engineering Department, Stanford University, Stanford, California, USA.

We then combine the cosmic ray secondary distributions with the effective seeding calculations to determine the effective flux of seed particles relevant to RREA initiation as a function of altitude.

2. Cosmic Ray Secondary Particle Distributions

[6] Cosmic rays have been studied extensively, with the main properties well characterized. The distribution of primary cosmic rays with energies above a few GeV is known to high precision over many orders of magnitude in energy, falling roughly as $dN_p/d\mathcal{E} \propto 1/\mathcal{E}^3$ with slight deviations [e.g., *Wolfendale*, 1973; *Nagano and Watson*, 2000]. For primary energies below a few GeV, the distribution is time-dependent and latitude-dependent but drops off rapidly as lower-energy primaries are deflected by the geomagnetic or heliomagnetic fields [*Jursa*, 1985]. When a primary cosmic ray hits the upper atmosphere, it generates a shower of secondary particles called an extensive air shower (EAS) with a maximum number of secondary particles roughly proportional to the primary energy, $dN_s/dN_p \propto \mathcal{E}$.

[7] Given only these rough proportionalities, it is useful to consider the total number of cosmic ray secondaries incident on some region of interest:

$$N_s \approx \int_{\mathcal{E}_{min}}^{\mathcal{E}_{max}} \frac{dN_s}{dN_p} \frac{dN_p}{d\mathcal{E}} d\mathcal{E} \propto \int_{\mathcal{E}_{min}}^{\mathcal{E}_{max}} \frac{1}{\mathcal{E}^2} d\mathcal{E}. \quad (1)$$

The $1/\mathcal{E}^2$ dependence in the integrand indicates that lower-energy cosmic ray primary particles on average contribute more secondary particles to a region of interest than higher-energy primaries. This dependence represents only a rough conceptual treatment, however. The actual secondary distributions in secondary energy, direction, and particle species are of course not captured in equation (1), nor is the critical question of the likelihood of various statistical fluctuations about the mean.

[8] To address these issues, we run Monte Carlo simulations of CR EASs using the AIRES software package (S. J. Sciutto, AIRES user's manual and reference guide, version 2.6.0, 2002, available at http://www.fisica.unlp.edu.ar/auger/aires/). For the purposes of computational efficiency, we have constructed a library of cosmic ray air shower data, simulating cosmic ray air showers for each point on a grid spanning a range of primary energies and incident zenith angles. At least 5 cosmic ray air showers are simulated at each point on the grid, with up to 20 showers simulated at lower energies. Primary energies are taken to range from 10^9 eV to 10^{15} eV with 4 steps per decade in energy, while incident zenith angles θ are taken from points uniformly spaced in $\cos\theta$ from $\cos\theta = 0.05$ to $\cos\theta = 0.95$ in steps of 0.1. Cosmic rays of energies below 10^9 eV have little influence on altitude ranges examined as the showers they produce do not sufficiently penetrate to high atmospheric depths. The mean number of cosmic ray primaries of energies above 10^{15} eV for the largest region and integration time considered here (8 km radius, 10 μs) is much less than unity. As we are focusing on the initial seeding processes before significant RREA, discharge, or feedback effects develop, this library spans the relevant range.

[9] The AIRES simulations of these primaries incident on the atmosphere are tracked at altitudes ranging from 1 km to 30 km and are used to fill histograms of the development of
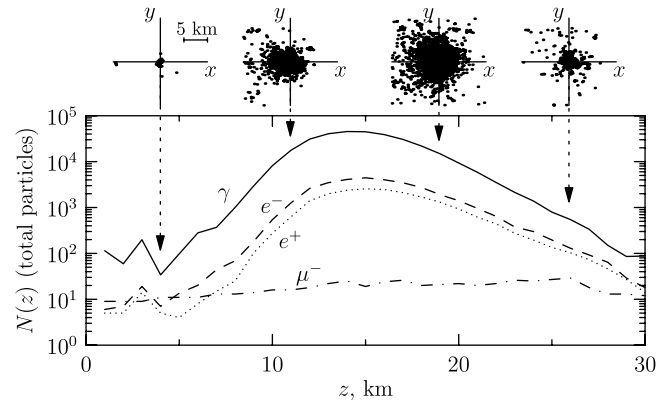

Figure 1. Sample cosmic ray secondary distributions shown for a 10^{13} eV primary with a zenith angle $\theta \sim 70°$ (cos $\theta = 0.35$). Number of secondary particles of various types versus z is shown in the main plot, with several x, y distributions in a plane perpendicular to and centered on the shower axis plotted over a $\pm$ 10 km range shown above for various z as indicated.

the associated air showers. The histograms show the distribution of each major type of secondary particle ($e^\pm$, $\mu^\pm$, γ) over energy and location in a plane perpendicular to the shower axis at each observing altitude. One such distribution is shown in Figure 1. Cosmic ray air shower data are subsequently taken from this library of histograms as appropriate instead of being resimulated.

[10] To calculate the distribution and fluctuations of the number of cosmic ray secondary particles, it is necessary to specify the geometry of the region of interest over which seeding may take place, i.e., the electric field region. Here, we consider spherical volumes of radius r ranging from 100 m to 3 km at altitudes ranging from 0.5 km to 29.5 km. The regions are taken to exist for the light travel time scale, r/c.

[11] We simulate the number of cosmic ray secondaries that intersect the region of interest by first simulating the number of primary cosmic rays that intersect a larger region enclosing the region of interest. This enclosing region is taken to have a radius 5 km larger than the radius of the region of interest as the typical size of a large EAS is less than 5 km so cosmic ray primaries not intersecting the enclosing region will not contribute significantly to the region of interest and can be neglected. The average integrated cosmic ray flux is used to calculate the mean number of primary cosmic rays that would intersect this enclosing region from above. The number of primary cosmic rays in each simulation is chosen as a Poisson random number with this mean. Each cosmic ray primary is then assigned an energy drawn randomly from the measured energy distribution as given by *Wolfendale* [1973], a direction drawn uniformly in solid angle, and an intersection point with the enclosing region drawn uniformly in area.

[12] The cosmic ray air showers resulting from these randomly chosen primaries are then drawn at random from the library entry for the primary cosmic ray nearest in energy and zenith angle to the random primary in question. As it is time consuming to draw and tabulate the extremely large numbers of cosmic ray showers that would intersect a
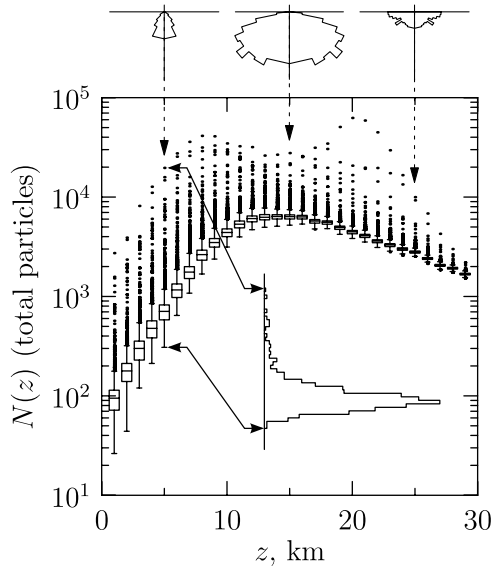
Figure 2. Distribution of total number of secondaries of all types incident on a 300 m radius sphere in 1 μs shown versus z, with statistical fluctuations over 1000 trials shown as box-whisker plots with a representative histogram for results at 5 km inset as indicated. Several directional distributions are shown in polar form (radius represents $dN/d\Omega$) above for 3 representative altitudes. Box-whisker plots shown are standard minimum/Q_1/median/Q_3/maximum (Q_1, Q_3 are the first and third quartiles), with dots shown for "outliers" defined as falling more than 1.5 (Q_3-Q_1) from the median.

large long-lived enclosing region, only up to 10^6 primary particles are included. If more than 10^6 primary particles were drawn to intersect the enclosing region, the results from the first 10^6 are scaled appropriately. This limit only applies to the largest and longest-lived regions of interest and acts to increase the fluctuation size above the true value. The distributions of cosmic ray secondaries incident on the region of interest are taken from the library histogram location bins that intersect the region of interest. These distributions of intersecting particles are then summed over all randomly chosen primaries, resulting in an overall particle type, energy, and direction distribution of secondary particles incident on the region of interest at each observing altitude.

[13] The distributions of secondaries calculated in this manner are subject to fluctuations of the total number of cosmic rays incident on the region, the energies of these cosmic rays, and the locations where the cosmic ray primaries were chosen to hit the enclosing region. These statistical fluctuations are fully captured in our analysis, though additional effects like the geographic dependence of the low-energy primary cosmic ray flux may have a small systematic effect. One such set of distributions is shown in Figure 2. These secondary particle distributions are a large portion of the information necessary to determine the number of seed particles for a RREA process. As a simple benchmark, compare our near sea level results from Figure 2 to well-known experimental results: the experimental and theoretical results give a total sea level flux of $\sim$300 m^{-2}s^{-1}sr^{-1} [*Kaye and Laby*, 1995], while the our

calculations give a flux of $\sim$250 m^{-2}s^{-1}sr^{-1} ($\sim$60 total particles incident on a region of interest of 300 m radius, 1 μs lifetime, and relevant solid angle range determined by the angular distribution of cosmic ray secondaries to be $\sim$1 sr). This relatively small discrepancy is likely due to the limits placed on our simulated primary energies.

3. Seeding Efficiency Simulations

[14] The cosmic ray secondary particle distributions do not directly give the effective number of RREA seed particles, however. Cosmic ray EASs typically consist of $\approx$89% photons, $\approx$10% electrons and $\approx$1% other particles, largely muons. These different particle types all result in different numbers of RREA seed electrons. Cosmic ray secondary particles moving at different directions relative to the driving electric field also seed RREA differently. Particles of different energies also clearly have different efficiencies for RREA seed electron production. These differences result from the different interaction cross sections for energetic electron production for various types of incident particle of various energies. Indirect processes (for example, involving intermediate particles or decay products) also result in different seeding efficiencies.

[15] We treat these difficulties by running simulations of the seeding process with the GEANT4 software package [*Agostinelli et al.*, 2003], which accounts for all relevant physical processes for all major particle species present in EAS. As we are not interested in the long-term development of the seed particle, but rather only in the production rate of RREA avalanche electrons, we limit the particles tracked in the simulation: the initial particles (the potential cosmic ray secondaries) are tracked for only 100 ns. To allow for a small amount of avalanche growth while limiting the growth of the total number of particles in the simulation, any secondary particles produced either by the initial particle or any secondary particles are tracked until 20 ns after the initial particle interaction that produced those secondaries. Results are shown for simulations with an electric field 1.5$\times$ the runaway breakdown threshold ($E_{th} \sim 270$ kV/m) [see, e.g., *Coleman and Dwyer*, 2006], but calculations at other typical electric fields up to a few times E_{th} (results not shown) indicate that electric field strength does not have a major effect on our results: as the electric field increases the threshold energy for RREA initiation decreases slightly and the possibility of initiation of RREA by positrons flowing in the direction of the electric field is enhanced but the overall shape and magnitude of the curves does not change. Simulations are executed for incident electrons, positrons, muons, and photons of various energies and directions relative to the electric field. Simulations are repeated 1000 times, and the average number of secondary avalanche particles (electrons and photons) present at the end of the simulations is calculated.

[16] These secondary particle counts are not directly physically meaningful, however, as they depend on the conditions and limits of the simulation. To convert the secondary counts to physical quantities, the number of secondary particles is normalized to the average number of secondary particles produced by a 1 MeV electron moving in the direction of avalanche growth, i.e., a typical avalanche electron.
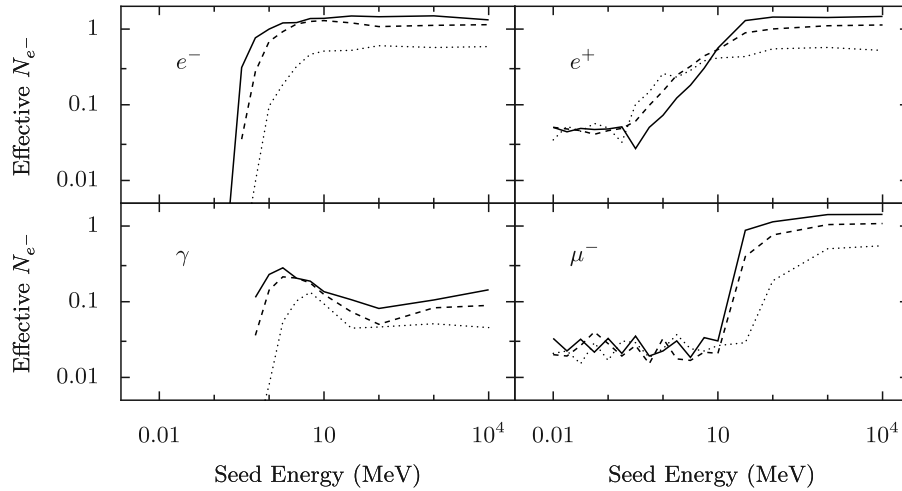
Figure 3. Effective number of downstream 1 MeV seed electrons versus initial particle energy for various seed particle types, energies, and directions. Seed particle momentum in direction of avalanche growth (downstream) shown in solid lines, perpendicular (cross-stream) shown in dashed lines, and opposite (upstream) shown in dotted lines.

[17] The results are shown in Figure 3. The efficiency varies substantially over the energy range examined, largely because of threshold effects as low-energy seed particles cannot produce relativistic particles for RREA. Notable exceptions to this threshold effect are positrons and muons, which can produce decay and annihilation products of sufficient energy to induce RREA. Initial particles traveling in the direction opposite the electric field (i.e., downstream in the direction of RREA growth) are typically a few times more efficient than initial particles traveling in the direction of the electric field (upstream) as it is more efficient to produce secondaries with downstream-directed velocities, though the acceleration of medium-energy upstream-directed positrons can offset this disadvantage. These efficiency results can then be combined with the cosmic ray secondary particle distributions to calculate the effective number of downstream 1 MeV avalanche electrons relevant to the region of interest.

4. Effective Seeding Results

[18] The distributions of cosmic ray secondary particles described above can easily be combined with the seeding efficiency calculations. Each bin (particle type, energy, direction) in the cosmic ray secondary particle histograms is multiplied by the appropriate factor from the seeding efficiency simulation results to obtain the effective number of initial downstream 1 MeV RREA electrons. These results, including variation induced by fluctuations in the total cosmic ray secondary distributions, are shown in Figure 4.

[19] The final effective seeding results are qualitatively similar to the cosmic ray secondary particle distributions, indicating that the subtleties of RREA seeding efficiency do not play a major role, but that the effective number of RREA seeds is substantially smaller than would be expected from a one to one translation from total cosmic ray secondary particles to RREA seed electrons and slightly smaller than the number of CR secondary electrons.

[20] A rough conversion to approximate the results of the combination of the seeding efficiency calculations with

cosmic ray secondary distributions to facilitate calculation of effective seed populations is: 0.5 to 1 RREA seed electrons are produced per cosmic ray secondary electron when energy, direction, and all major CR secondary particle types are taken into account.

5. Discussion

[21] The above results lead to two main conclusions. First, that the effective number of seed electrons received
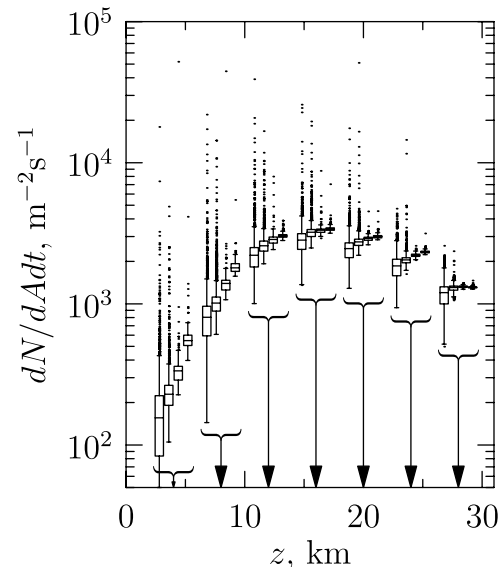

Figure 4. Effective number of 1 MeV downstream RREA electrons produced within a volume of interest per area per time shown versus altitude for four different regions of interest grouped by curly braces indicating the altitude of the regions of interest. Within each group the regions of interest are, from left to right, 100 m/0.3 μs, 300 m/1 μs, 1 km/3 μs, 3 km/10 μs. Box-whisker plots are standard (see Figure 2 caption).

by a volume relevant to RREA is large. Second, that while the fluctuations can be substantial, they are seldom larger than 10 times the typical number.

[22] The large number of seed electrons implies that a region of electric field in the Earth's atmosphere does not need to wait long for the presence of seed particles to initiate RREA: for the regions considered here, the first RREA seed particles will appear within 1 μs of the formation of the electric field. Thereafter, RREA will occur as the population of seed particles is amplified. This result implies that the presence of RREA essentially tracks the presence of the driving electric field, though this does not specify the global significance of the RREA seeding. Careful consideration must be made of the importance of the RREA seeding, as geometric limits to the avalanche may prevent the growth of even a large seed population, while feedback effects may circumvent the requirement of large seed populations [see *Dwyer*, 2003, 2007]. Here we only state that the seed population is nontrivial.

[23] The scale of the fluctuations indicates that while it may be tempting to suggest that rarely observed processes such as terrestrial gamma ray flashes are caused by rare coincidence of intense electric fields and large fluctuations in the number of RREA seed particles, such explanations need to very carefully consider the size of fluctuation required, the frequency of such fluctuations, the relative importance of the background seed population present without fluctuation, and the possible RREA amplification of this background seed population. The possibility of selection bias in the observation of the effects of RREA will further complicate this analysis and unfortunately precludes any globally valid statements about the significance of the size of the fluctuations.

[24] Future work should focus on integrating these results with electrodynamics and RREA simulations to better understand the interaction of the electric field source, the seeding process, and RREA dynamics to produce the resulting observables. Detailed statistical analysis of these processes can answer questions about the feasibility and occurrence frequency of processes relying on large CR EAS or otherwise large fluctuations in the seed population.

References

Agostinelli, S., et al. (2003), G4: A simulation toolkit, *Nucl. Instrum. Methods Phys. Res., Sect. A*, *506*(3), 250–303.

Babich, L. P., E. N. Donskoy, I. M. Kutsyk, and R. A. Roussel-Dupré (2005), The feedback mechanism of runaway air breakdown, *Geophys. Res. Lett.*, *32*, L09809, doi:10.1029/2004GL021744.

Babich, L. P., A. Y. Kudryavtsev, M. L. Kudryavtseva, and I. M. Kutsyk (2007), Terrestrial gamma-ray flashes and neutron pulses from direct simulation of gigantic upward atmospheric discharge, *J. Exp. Theor. Phys. Lett.*, *85*(10), 483–487, doi:10.1134/S0021364007100037.

Coleman, L. M., and J. R. Dwyer (2006), Propagation speed of runaway electron avalanches, *Geophys. Res. Lett.*, *33*, L11810, doi:10.1029/2006GL025863.

Dwyer, J. R. (2003), A fundamental limit on electric fields in air, *Geophys. Res. Lett.*, *30*(20), 2055, doi:10.1029/2003GL017781.

Dwyer, J. R. (2005), The initiation of lightning by runaway air breakdown, *Geophys. Res. Lett.*, *32*, L20808, doi:10.1029/2005GL023975.

Dwyer, J. R. (2007), Relativistic breakdown in planetary atmospheres, *Phys. Plasmas*, *14*(4), 042901, doi:10.1063/1.2709652.

Dwyer, J. R., and D. M. Smith (2005), A comparison between Monte Carlo simulations of runaway breakdown and terrestrial gamma-ray flash observations, *Geophys. Res. Lett.*, *32*, L22804, doi:10.1029/2005GL023848.

Gurevich, A. V., and K. P. Zybin (2001), Runaway breakdown and electric discharges in thunderstorms, *Phys. Usp.*, *44*(11), 1119–1140, doi:10.1070/PU2001v044n11ABEH000939.

Gurevich, A. V., and K. P. Zybin (2004), High energy cosmic ray particles and the most powerful discharges in thunderstorm atmosphere, *Phys. Lett. A*, *329*, 341–347, doi:10.1016/j.physleta.2004.06.094.

Gurevich, A. V., G. M. Milikh, and R. A. Roussel-Dupré (1992), Runaway mechanism of air breakdown and preconditioning during a thunderstorm, *Phys. Lett. A*, *165*, 463–468, doi:10.1016/0375-9601(92)90348-P.

Gurevich, A. V., K. P. Zybin, and R. A. Roussel-Dupré (1999), Lightning initiation by simultaneous effect of runaway breakdown and cosmic ray showers, *Phys. Lett. A*, *254*, 79–87, doi:10.1016/S0375-9601(99)00091-2.

Inan, U. S., and N. G. Lehtinen (2005), Production of terrestrial gamma-ray flashes by an electromagnetic pulse from a lightning return stroke, *Geophys. Res. Lett.*, *32*, L19818, doi:10.1029/2005GL023702.

Jursa, A. S. (Ed.) (1985), *Handbook of Geophysics and the Space Environment*, Air Force Geophys. Lab., Air Force Syst. Command, Springfield, Va.

Kaye, G., and T. Laby (1995), *Tables of Physical and Chemical Constants*, Longman, New York.

Lehtinen, N. G., M. Walt, U. S. Inan, T. F. Bell, and V. P. Pasko (1996), γ-ray emission produced by a relativistic beam of runaway electrons accelerated by quasi-electrostatic thundercloud fields, *Geophys. Res. Lett.*, *23*, 2645–2648.

Lehtinen, N. G., T. F. Bell, and U. S. Inan (1999), Monte Carlo simulation of runaway MeV electron breakdown with application to red sprites and terrestrial gamma ray flashes, *J. Geophys. Res.*, *104*, 24,699–24,712, doi:10.1029/1999JA900335.

Marshall, T. C., M. Stolzenburg, C. R. Maggio, L. M. Coleman, P. R. Krehbiel, T. Hamlin, R. J. Thomas, and W. Rison (2005), Observed electric fields associated with lightning initiation, *Geophys. Res. Lett.*, *32*, L03813, doi:10.1029/2004GL021802.

Nagano, M., and A. A. Watson (2000), Observations and implications of the ultrahigh-energy cosmic rays, *Rev. Mod. Phys.*, *72*, 689–732.

Roussel-Dupré, R. A., and A. V. Gurevich (1996), On runaway breakdown and upward propagating discharges, *J. Geophys. Res.*, *101*, 2297–2312, doi:10.1029/95JA03278.

Tierney, H. E., R. A. Roussel-Dupré, E. M. D. Symbalisty, and W. H. Beasley (2005), Radio frequency emissions from a runaway electron avalanche model compared with intense, transient signals from thunderstorms, *J. Geophys. Res.*, *110*, D12109, doi:10.1029/2004JD005381.

Wolfendale, A. W. (Ed.) (1973), *Cosmic Rays at Ground Level*, Inst. of Phys., London.

————————
B. E. Carlson, U. S. Inan, and N. G. Lehtinen, Space, Telecommunications, and Radioscience Laboratory, Electrical Engineering Department, Stanford University, 350 Serra Mall, Packard Building, Stanford, CA 94305-9515, USA.